

This is a preprint version of the article published in:
Journal of Sound and Vibration, Vol. 409, pp. 112-130 (2017).
<http://dx.doi.org/10.1016/j.jsv.2017.07.047>

Please, cite this document as:

T. G. ZIELIŃSKI. "Microstructure representations for sound absorbing fibrous media: 3D and 2D multiscale modelling and experiments." *Journal of Sound and Vibration*, Vol. **409**, pp. 112-130 (2017).

DOI: [10.1016/j.jsv.2017.07.047](https://doi.org/10.1016/j.jsv.2017.07.047)

Microstructure representations for sound absorbing fibrous media: 3D and 2D multiscale modelling and experiments

TOMASZ G. ZIELIŃSKI

Institute of Fundamental Technological Research, Polish Academy of Sciences
ul. Pawinskiego 5B, 02-106 Warsaw, Poland
e-mail: tzielins@ippt.pan.pl

Abstract

The paper proposes and investigates computationally-efficient microstructure representations for sound absorbing fibrous media. Three-dimensional volume elements involving non-trivial periodic arrangements of straight fibres are examined as well as simple two-dimensional cells. It has been found that a simple 2D *quasi*-representative cell can provide similar predictions as a volume element which is in general much more geometrically accurate for typical fibrous materials. The multiscale modelling allowed to determine the effective speeds and damping of acoustic waves propagating in such media, which brings up a discussion on the correlation between the speed, penetration range and attenuation of sound waves. Original experiments on manufactured copper-wire samples are presented and the microstructure-based calculations of acoustic absorption are compared with the corresponding experimental results. In fact, the comparison suggested the microstructure modifications leading to representations with non-uniformly distributed fibres.

Key words: sound absorption, fibrous materials, multiscale modelling, microstructure representations.

Highlights:

- Periodic 3D and 2D representations for sound absorbing fibrous media are proposed.
- Fibrous samples are manufactured and used to validate modelling.
- An agreement between 3D and 2D representations is demonstrated.
- A change in absorption due to a modification of fibre cross-section is predicted.

1. Introduction

Sound propagation and absorption in air-saturated porous media with sufficiently stiff frame can be predicted using the so-called Johnson-Champoux-Allard (JCA) model [1–3] or its enhanced versions involving some improvements concerning viscous dissipation [4] and thermal effects [5–7]. Namely, Pride *et al.* [4] proposed a correction for the imaginary part of dynamic viscous permeability which is underestimated at low frequencies by the original Johnson-Koplik-Dashen model [2], whereas corrections for thermal effects involved introduction of a static thermal tortuosity [5] and a thermal analogue of permeability [6]. Finally, what resulted are precise semi-phenomenological models with rather large number of parameters, involving in the most advanced case: the open porosity, the (inertial) tortuosity, the static viscous permeability and its thermal analogue, the viscous and thermal characteristic lengths, and the static viscous and thermal tortuosities. Simpler phenomenological models do exist, in particular, the purely empirical models by Delany and Bazley [8] with important corrections and generalizations by Miki, namely: a correction for low frequencies [9], and a generalisation introducing porosity and tortuosity [10]. They are valid for some fibrous absorbent materials of very high porosity (originally they were proposed and validated for fibrous materials with porosity close to unity). The main material parameter is here the flow resistivity of fibrous material. More recently, an improved empirical model for fibrous materials was proposed by Voronina [11]. In general, more complex, general models (especially, the mentioned JCA model or its enhanced versions) are less restrictive, yet they involve many parameters related to the average geometry of porous or fibrous media. These parameters (usually referred to as *transport parameters*) can be in fact determined from microstructure of a porous (or fibrous) medium, and it seems that soon such microstructure-based approach should allow to design and optimise novel acoustic materials. Improvements in robust passive acoustic treatments are possible, although an active approach has been proposed [12].

Realistic microstructure-based calculations become now an important tool for prediction of attenuating performance of sound absorbing porous and fibrous media. Such an approach has been recently applied to various porous materials, namely: to open-cell aluminum foams [13, 14], to perforated closed-cell metallic foams [15], to open-cell foams with microstructure represented by idealised packing of polyhedral periodic unit cells [16], to a fibrous material with hexagonal arrangement of fibres [17], to open-porosity ceramics [18] and other open-cell foams with spherical pores [19], to polyurethane foams in order to optimise their low frequency sound absorption by cell size control [20], to granular media with face-centred cubic packing [21] and also other packings of spherical grains [22, 23], to granular media with double porosity [24], and to double porosity foams [25]. Moreover, various microstructure-based analyses have been also applied when studying wave propagation in poroelastic materials [26–29].

Nevertheless, the accuracy of such calculations strongly depends on a correct choice of representative micro-structural geometry of porous media, and that choice is constrained by some requirements, like: the periodicity, a relative simplicity of micro-geometric representations, and the size of elementary volume (or cell) which should be small enough to allow for the separation of scales [30].

One of important transport parameters is the static viscous permeability, and in particular, a dynamic generalisation of this parameter: the frequency-dependent and complex-valued dynamic permeability [2]. It was investigated by Johnson *et al.* [2], and also, for example, by Cortis and Berryman [31] in case of frequency-dependent viscous flow in channels with rough surfaces. The real part of this frequency-dependent function of dynamic permeability converges to the value of static permeability when the frequency tends to zero. Thus, the parameter of Darcy permeability forms a low-frequency limit of its dynamic generalisation, and therefore, it is used as an important reference parameter in the analytical approximating formulas for the dynamic permeability [1, 2]. Microstructural influences on the permeability of fibrous media have been studied by many authors, for example: for media with uni- and bi-modal fibre size distribution [32, 33], in case of 2D periodic fibrous representations [34], and using 3D imaging coupled with CFD simulations [35]. The role of microstructural parameters in radiative heat transfer through disordered fibrous media was investigated by Tahir *et al.* [36]. Koponen *et al.* [37, 38] used the lattice-Boltzmann methods to study the interdependence of permeability, tortuosity, and porosity of random fibrous media. They confirmed that permeability exponentially depends on porosity over a large range of porosity, and proposed a modification of the Kozeny-Carman equation for permeability by involving the concept of effective porosity. Tomadakis and Robertson [39] compared diffusional and electrical estimates of viscous permeability and tortuosity of random fibre structures with analytical formulas and experimental results.

The acoustic attenuation of sound absorbing fibrous materials strongly depends on the dynamic resistivity to an oscillating air flow, which is directly related to the dynamic permeability. This matter was studied by Tarnow [40], who calculated the dynamic resistance for a 2D model of randomly placed cylinders (discs) with geometry simulating the geometry of a real fibrous material. Earlier, the same author [41] investigated the dynamic compressibility of air in fibrous materials, which was determined for 2D models with parallel cylinders: placed in a regular square lattice and placed randomly. Tarnow carried out also experimental investigations on the sound propagation in glass wool [42], and later in particular, he investigated the effect of fibre movements on the sound attenuation in this material [43].

Schladitz *et al.* [44] presented a method of design for a stacked fibre non-woven acoustic trim based on geometric modelling and flow simulations. The non-woven fabric was modelled by a macroscopically homogeneous random system of straight cylinders (tubes). Such geometric model was generated from stochastic geometry (obtained using image acquisition) by adapting the characteristic properties of the material (i.e., porosity, fibre size distribution). For the geometric model, the Stokes equations were solved with no-slip boundary conditions on fibre surfaces using the generalized lattice Boltzmann method. Numerical calculations allowed to determine the flow resistivity of the material, which was then used in the formulas of Delany–Bazley model [8] improved for low frequencies by Mechel [45] to predict the frequency-dependent acoustic absorption (these final

results were confronted with measurements). The authors proposed a design procedure for a non-woven material with improved acoustic absorption properties as follows. First, the fibre thickness, porosity and anisotropy of the fibre system are modified. Then, the flow and acoustic simulations are performed for the new geometric sample. These two steps are repeated for various sets of parameters. Finally, the set of parameters for the geometric model leading to the best acoustic absorption is found.

Thermoacoustic properties of fibrous materials were studied by Jensen and Rasmussen [46]: they used computational fluid simulations to test the proposed models for propagation in porous materials with an ambient temperature gradient. These authors also used the lattice Boltzmann model for flow simulations and the geometric model used for the fibrous material was the same as the one used by Schladitz *et al.* [44].

The effect of some physical parameters on sound absorption properties of natural fibre mixed non-woven composites was studied experimentally by Küçük and Korkmaz [47]. Along with the sound absorption properties they measured thickness, weight per unit area, and air permeability for samples of eight different non-woven composites including different fibre types mixed with various ratios (for example, 70% of cotton and 30% of polyester fibres). They found in particular for such composites that the increase in amount of fibre per unit area resulted in an increase in sound absorption of the material. (Of course, it is within some reasonable limit of fibre amount, since on the other hand, too many fibres may eventually make the airflow resistivity too large and degrade the sound absorption.)

Determination of a representative volume element of random fibrous media suitable for estimation of their acoustic properties was studied by Peyrega and Jeulin [48, 49]. As a matter of fact, a random fibrous medium was modelled in this study in a fairly simplified way, namely, in the form of infinite straight parallel fibres set along the surface plane normal to the acoustic waves penetrating the medium. Thanks to this assumption, the medium could be represented as a periodic array of circular cylinders (PACC), or in fact, as a two-dimensional array of circular discs. The authors generated numerous independent 2D realisations of PACC composed of overlapping fibres in accordance with the Boolean model, as the result of the location of the centres of discs, according to a random Poisson point process [50]. The work presents the results of numerical thermo-acoustic simulations based on the 2D random representations of fibrous media (where the circular discs are allowed to overlap), although in the initial part of work the curves of acoustic absorption computed using 2D PACC representations are compared with some available measurements of a fibrous material (see Figure 4 in Ref.[48]).

The present work discusses the microstructure-based approach involving the visco-thermo-acoustic calculations for sound absorbing fibrous media with respect to the important issue of Representative Volume Elements (RVEs). In particular, truly 3D and eventually also 2D representations for a fibrous material made up of a metal wire are proposed, studied and validated experimentally. The paper is organised as follows. First, a methodology of manufacturing of fibrous samples from a copper wire is described and the measurements of sound absorption for a few layers of such fibrous material of various thickness are presented. Next, three-dimensional periodic arrangements of fibres are discussed and proposed as suitable for volume elements of fibrous media. Combinations of these arrangements are then used to construct a couple of periodic volume elements and the multi-scale analyses involving the relevant microstructure-based computations are carried out on these RVEs. Eventually, also a two-dimensional representative cell is proposed and used for micro-structural calculations. The results of micro-structural analyses serve to determine the effective speed of sound and effective density for fibrous media of the proposed micro-geometry and to compute the acoustic wave velocity in such media. All this allows to calculate the acoustic absorption coefficient for layers of various thickness and compare these results with the measurements obtained for the fibrous samples. In the final part of paper, some additional numerical and experimental studies are discussed – to demonstrate and verify the correctness of the proposed computationally economical approach based on *quasi*-representative two-dimensional cells for fibrous media. These studies concern a fibrous material made up from oblate wire – manufactured from the round wire used previously, so that the effect of cross-section change is clearly predicted.

2. Manufacturing and experimental testing of fibrous samples

Several fibrous samples were manufactured from a silver-plated copper wire of diameter 0.5 mm. The samples were manually braided from 10 cm long pieces of wire and they were fitted into the impedance tube of diameter 29 mm (see Figure 1). In that way the samples were shaped into cylinders. As a matter of fact, in the process of manufacturing each sample was being inserted into the tube and taken out of it many times, so that some new wire fibres could be pierced and interwoven through the sample; as a result lengthy parts of wires are straight and the samples are macroscopically homogeneous along their lengths and with respect to their both ends, which was later confirmed in a way by experiments.

In particular, two fibrous samples were manufactured: one has a height of 30 mm and the other one is two times higher (see Figure 2). The total length of wire used for the smaller sample is 10 m, and for the twice taller one it is 20 m, so that both samples have the same porosity of 90%.

The samples were tested in the impedance tube using the two microphone transfer function method [51]. The acoustic absorption coefficient was measured in the frequency range from 500 Hz to 6.4 kHz during 12 different experimental tests, namely:

- 2 tests of the smaller sample set on the rigid termination in the tube: with one face (side) exposed to penetrating acoustic waves, and then, the other way around;
- 2 similar tests of the larger sample;

- 4 tests when both samples are put inside the tube – the larger sample directly behind the smaller one, so they form a double layer with thickness 30 mm + 60 mm = 90 mm (4 tests were carried out to realize all possible face-to-face configurations);
- 4 similar tests (as above), but this time the smaller sample is set behind the larger one, and the total thickness is also 90 mm = 60 mm + 30 mm.

Acoustical measurements carried out on all manufactured fibrous samples in the impedance tube proved repeatability of the proposed preparation technique. Figure 3 presents some of the experimental results for the fibrous samples with porosity 90%.



Figure 1: Manufacturing of a fibrous sample from 10 cm long pieces of copper wire with diameter 0.5 mm, and the sample inside the impedance tube with diameter 29 mm

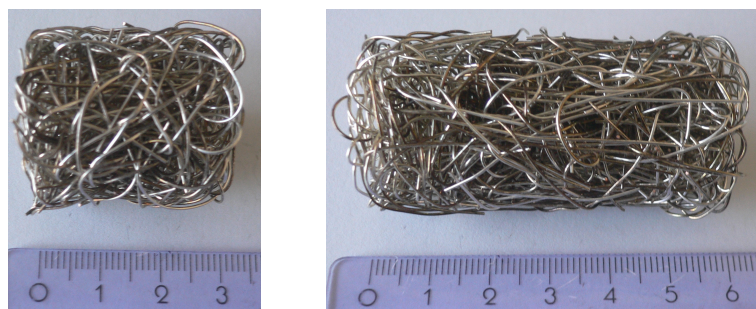


Figure 2: Two fibrous samples with porosity 90%, manufactured from the copper wire of diameter 0.5 mm; both samples are cylindrical in shape with diameter 29 mm and heights: 30 mm or 60 mm

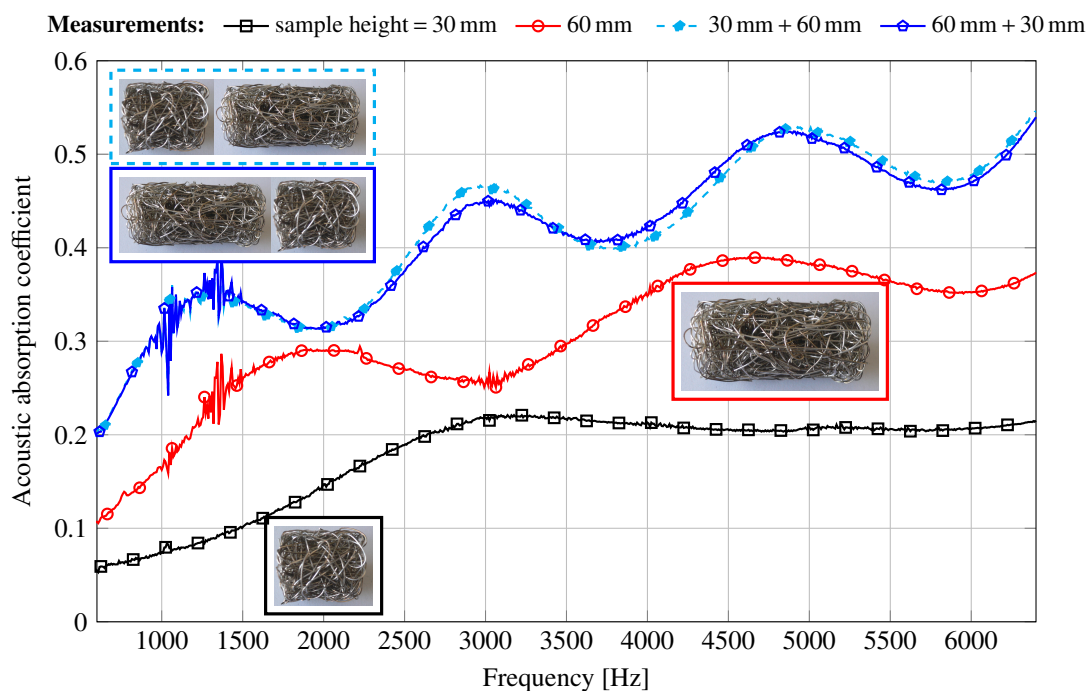


Figure 3: Sound absorption measured in the impedance tube for the fibrous samples manufactured from the copper wire

The absorption curves obtained for different side-configurations were always practically identical, and so only one representative curve is plotted for each case. It proves that the technique of sample preparation is good, which is even more confirmed when the comparison is made between the results obtained for two different double-layered cases: the sound absorption measured when the small sample was in front of the large one is almost identical to the result when they were put the other way around! – both curves are plotted in Figure 3 to show how small are the discrepancies. Thus, both samples – the small and the large one – have *not only* the same porosity and fibre diameter but also statistically-identical geometry of microstructure.

3. Periodic arrangements of fibres

In this Section some simple (though, not trivial) fibrous arrangement will be proposed as a possible representation for the fibrous geometry of wire samples. The proposition will be based on two facts concerning the technique used for sample preparations, namely: (1) the samples were braided from long wires which were rather mildly bent; (2) many of them pierced through the whole fibrous sample to be bent mildly around and pierce again inside. Therefore, there are two main assumptions consistent with these facts: (1) locally, the fibres are straight; (2) the fibres pass through the volume element, that is, no fibre endings appear in the cell. There is also an obvious requirement that the porosity of a fibrous representative cell must be equal to the porosity of fibrous samples, which is 0.90. Accordingly, the thermal characteristic length, which is a generalisation of the hydraulic radius, will also characterise the proposed simplified representations of microstructure. It is defined as the doubled volume of fluid domain to the surface of (wetted) solid walls, and for the samples with porosity 0.90 and manufactured from round wire with diameter 0.5 mm, this value can be easily estimated as 2.27 mm, or in fact, a bit less than that value since the wire is in pieces and the cut-wire endings increase slightly the wetted solid surface. Moreover, all representative volume elements or cells proposed in this work satisfy the fundamental mathematical requirement that the arrangement of fibres in cells is periodic (although, symmetric conditions could also be used).

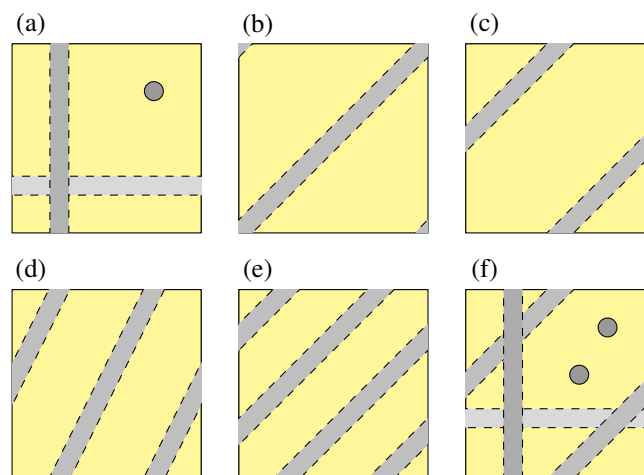


Figure 4: Generic periodic arrangements of straight fibres in the representative cube: (a) three mutually-perpendicular fibres normal to the adequate faces of the cube; (b, c, d, e) mutually-parallel fibres set obliquely to four faces of the cube and in the plane parallel to the remaining two faces; (f) an example of periodic cube with six fibres, two of them oblique

Here, the periodicity of non-trivial arrangements of fibres in a cubic or cuboid cell will be discussed. Figure 4 shows some periodic arrangements of fibres in a cubic (or cuboid) volume element on the viewing plane perpendicular to the direction of propagation. The straight fibres normal to some of the cube faces (and consequently, parallel to the remaining faces) – as shown in Figure 4(a) – can be added one by one to the volume element and the periodicity will always be maintained. This is *not* the case of oblique fibres. For simplicity, only such oblique fibres are considered which are lying in planes normal to the direction of propagation. For example, when a diagonal fibre is present, which passes through two corners of the cross-sectional square as depicted in Figure 4(b), the complementing fibre pieces appear in two remaining corners. When a slanting fibre is added, which passes through the middles of two neighboring edges of the square cross-section, a similar piece of fibre must be put symmetrically in the same plane to pass the opposite neighboring edges – such arrangement is shown in Figure 4(c). Adding an oblique fibre such as any of three fibres presented in Figure 4(d) requires also the presence of the other two fibres, and when a fibre is put like any of four fibre pieces shown in Figure 4(e) also the remaining three pieces must be added in order to satisfy the periodicity of arrangement. A periodic arrangements of oblique fibres can be of course combined with fibres parallel (or normal) to the volume element faces – a simple example with six fibres is given in Figure 4(f). However, more fibres in the representative volume element (with some prescribed porosity) means that its relative size must be increased and the straight fibres become longer (i.e., more slender) in order to preserve the assumed porosity, which is the most fundamental feature.

Figure 5 presents a cubic volume element which may be representative for the copper-wire fibrous material tested experimentally. The proposed cubic RVE contains four straight fibres in a uniformly-spaced configuration: three of them are perpendicular to the direction of propagation X , and one is parallel. Although, there is no full identity in arrangement between the X - and Y -

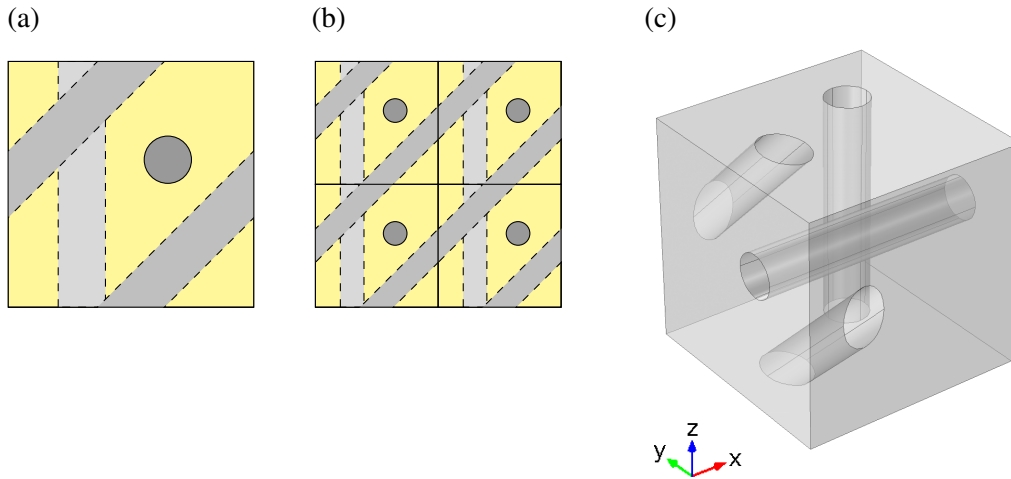


Figure 5: Fibrous Representative Volume Element *RVE-1* with a periodic arrangement of four regularly-spaced fibres and porosity 90%: (a) the *X*-normal view of a single periodic cubic cell; (b) the *X*-normal view of a set of four periodic cubic cells; (c) an axonometric view of the periodic cubic cell

or *Z*-direction, the uniform distribution of fibres should – in this case – set the macroscopic features of volume element close to isotropy. (In fact, most of real fibrous media tend rather to be transversally isotropic, and this feature will be characteristic for the other fibrous representations proposed further in this work.) The porosity of the fibrous volume element is exactly 90% which conforms with the porosity of copper-wire samples. In the next sections the multiscale modelling will be applied in order to check the degree of representativeness of this cubic volume element for the copper-wire fibrous material, and to eventually propose some simple modifications which should allow to take into account some prominent features missing in this element.

4. Multiscale analyses based on various representations

4.1. Multiscale modelling of sound absorbing fibrous media

The fibrous material from a thick, and therefore, stiff copper wire can be modelled using the assumption of frame (fibre) rigidity and motionlessness, which allows for the so-called fluid-equivalent approach. The *effective* density and bulk modulus for a porous (fibrous) medium modelled as an equivalent fluid are complex and frequency-dependent functions, i.e., $\varrho_e = \varrho_e(\omega)$ and $K_e = K_e(\text{Pr}\omega)$, respectively, where ω is the angular frequency and *Pr* is the Prandtl number. According to the well-known Johnson-Champoux-Allard (JCA) model they can be determined as follows [1]:

$$\varrho_e(\omega) = \frac{\alpha(\omega) \varrho_f}{\phi}, \quad K_e(\text{Pr}\omega) = \frac{K_f}{\phi \beta(\text{Pr}\omega)}, \quad \text{with} \quad \beta(\text{Pr}\omega) = \gamma_f - \frac{\gamma_f - 1}{\alpha'(\text{Pr}\omega)}. \quad (1)$$

Here, ϱ_f , K_f , γ_f , are the density, the adiabatic bulk modulus and the ratio of specific heats for pore-fluid (air), respectively, whereas $\alpha(\omega)$ and $\alpha'(\text{Pr}\omega)$ are the so-called viscous and thermal dynamic tortuosity functions. They describe some resistive effects of tortuous porous geometry to harmonically-driven viscous flow and thermal transport, respectively. Their meaning is different and in fact they are derived in a different way. The viscous tortuosity function $\alpha(\omega)$ depends on the kinematic viscosity of pore-fluid (air). The thermal tortuosity function $\alpha'(\text{Pr}\omega)$ depends on the thermal diffusivity, which is usually denoted as the kinematic viscosity divided by the Prandtl number *Pr*.

Since both tortuosity functions are in fact essentially related to the porous (fibrous) geometry, they can be expressed with semi-phenomenological formulas involving some *transport parameters* directly related to that geometry. Different variants of the Johnson-Champoux-Allard (JCA) model [1–3] employ various numbers of such parameters. The most complex Johnson-Champoux-Allard-Pride-Lafarge (JCAPL) model [1, 6] employs 8 transport parameters, namely: the open porosity ϕ , the (inertial) tortuosity α_∞ , the (viscous) permeability k_0 and its thermal analogue k'_0 , the viscous and thermal characteristic lengths Λ and Λ' , respectively, and the viscous and thermal static tortuosities α_0 and α'_0 , respectively. In fact, in this model the formula for $\alpha(\omega)$ employs: ϕ , α_∞ , k_0 , Λ , and α_0 , whereas the formula for $\alpha'(\omega)$ employs only: ϕ , k'_0 , Λ' , and α'_0 .

The transport parameters can be found from a representative geometry of porous (fibrous) microstructure. The porosity ϕ is directly obtained or known *a priori* as the most fundamental feature of any porous geometry. Also, the thermal characteristic length Λ' is determined directly from geometry as the doubled ratio of the fluid domain to the surface of solid frame (fibres) in a representative cell. The viscous permeability k_0 is calculated from the solution of the *scaled* Stokes problem of viscous incompressible flow through a periodic representative cell (in the direction of wave propagation) with the no-slip boundary conditions on the solid frame, i.e., on the fibres' surfaces. As a result a scaled (to the dimension of permeability) field of velocity is obtained, defined in the fluid domain; its averaging over the cell volume provides the viscous permeability parameter k_0 .

Another averaging formula allows to calculate the static viscous tortuosity α_0 . Similarly, the thermal analogue of permeability k'_0 and the static thermal tortuosity α'_0 are computed by averaging the solution of the *scaled* heat transfer problem in the fluid domain of a periodic representative cell with the isothermal boundary conditions on the surface of solid frame (fibres) – which can be considered as a thermostat having much higher thermal conductivity than the air. The scaling of the problem results in fact in the Poisson's equation and the solution is a field of temperature scaled to the dimension of permeability. Finally, the classic parameter of (inertial) tortuosity α_∞ and the viscous characteristic length Λ are calculated using averaging formulas applied to the solution of the Laplace problem. This problem results from a high-frequency limit of viscous flow where it becomes formally equivalent to the problem of electric conduction through a fibrous periodic cell filled with a conductive fluid and electrically-insulating fibres [52]. In the following Sections, the transport parameters will be calculated (in the ways discussed here) for three different periodic representations of fibrous microstructure with porosity 90% and fibre diameter 0.5 mm, namely: two volume elements and a two-dimensional cell. Then, they will serve to determine the tortuosity functions, effective properties and overall sound propagation and absorption for the investigated fibrous material. A similar hybrid (micro-macro) approach has been used, for example, in Refs. [14, 17, 21–23].

4.2. Analyses using a cubic RVE

The cubic volume element *RVE-1* with porosity 90% containing four uniformly-spaced fibres with diameter 0.5 mm (see Figure 5; the propagation direction is X) was used to solve the periodic finite element analyses discussed above. The solutions – the scaled velocity (or viscous permeability field), the scaled temperature (or thermal permeability field), and the scaled field of electric potential – are shown in Figure 6. They were used by the appropriate averaging formulas to calculate the transport parameters which are given for *RVE-1* in Table 1. These transport parameters permitted to determine the effective density and bulk modulus, and then, the effective speed of sound for a fibrous material represented on the micro-scale level by such a simple periodic arrangement of four straight fibres. In Section 4.5, the acoustic absorption coefficient calculated for a few layers of such fibrous material will be compared with the experimental results measured for the copper-wire samples to show that the proposed simple fibre geometry is rather weakly representative for them; however, important and obvious similarities between the corresponding computed and measured absorption curves encouraged some further developments as discussed below.

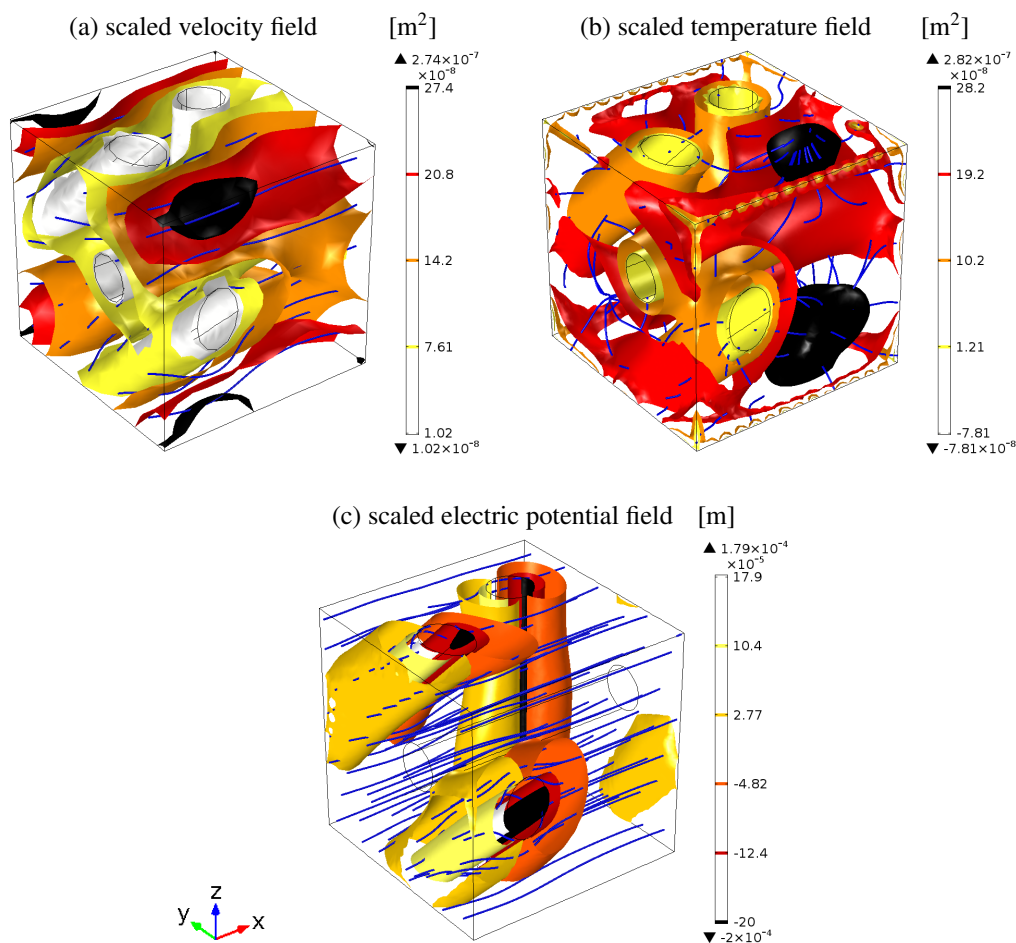


Figure 6: Solutions of microstructural problems in the fluid domain of the cubic fibrous representation *RVE-1*

Table 1: Transport parameters for various representations of the half-millimeter-wire fibrous material with porosity 90%

Parameter	Unit	RVE-1	RVE-2	Cell-2D
viscous permeability, k_0 :	$[10^{-9}\text{m}^2]$	116	73.9	48.7
thermal permeability, k'_0 :	$[10^{-9}\text{m}^2]$	156	483	204
(inertial) tortuosity, α_∞ :	[-]	1.07	1.10	1.12
viscous static tortuosity, α_0 :	[-]	1.38	1.47	1.30
thermal static tortuosity, α'_0 :	[-]	1.17	1.56	1.20
viscous charact. length, Λ :	[mm]	1.43	1.11	1.08
thermal charact. length, Λ' :	[mm]	2.27	2.26	2.25

4.3. Analyses using an elongated cuboid RVE

The discrepancies – reported below in Section 4.5 – between the direct experimental measurements and the results calculated from the cubic volume element *RVE-1* with uniformly-spaced fibres, suggested that the fibres in a representative geometry should be perhaps set more densely in order to improve the acoustic wave dissipation which was systematically underestimated in the calculations. Such concentrations of fibres would modify the throat size which controls the viscous permeability and therefore has a great impact on viscous effects. This conclusion was also supported by additional survey done to the actual microstructure of wire samples: in fact, at a closer look some distinct groupings of wire fibres could be observed. On the other hand, a very similar character of the corresponding measured and calculated absorption curves confirmed that the fundamental assumption of locally straight fibres is admissible. Therefore, another fibrous volume element was proposed, which in a different way combines the periodic arrangement of straight fibres discussed in Section 3. In this volume element most of fibres are grouped in a layer formed across the direction of propagation (which entails some sort of anisotropy at the macro-scale level). In fact, the volume element was elongated in that direction to form a periodic *cuboid*. It was constructed successively, by adding a few fibres at a time (the cuboid was at the same time relatively enlarged to maintain the porosity of 90%), doing all multiscale calculations and checking the final results with measurements. Such an approach gradually led to a better and better agreement between the numerical and experimental results. Finally, the fibrous volume element *RVE-2* presented in Figure 7 was attained. The relevant problems were solved in the fluid domain meshed with finite elements as shown in Figure 7 and the solution fields are shown in Figure 8. The corresponding values of transport parameters are listed in Table 1 for *RVE-2*. Before the results of wave speed, damping and sound absorption are presented for this representative volume element in Section 4.5, another proposition of microstructure representation in the form of a two-dimensional cell will be discussed.

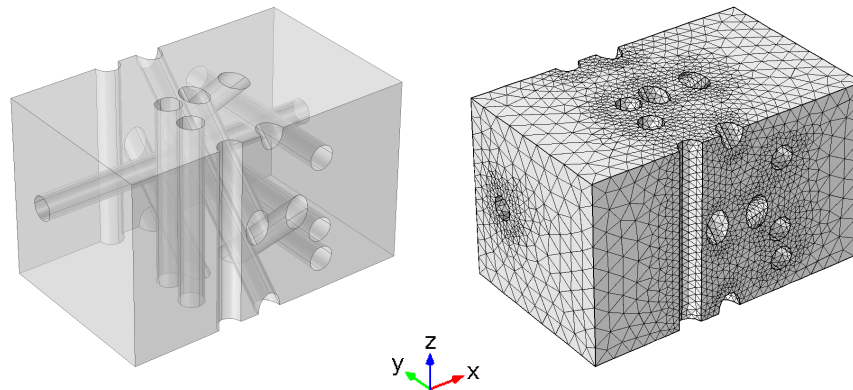


Figure 7: Fibrous Representative Volume Element *RVE-2* (and the corresponding finite element mesh) in the form of an elongated cuboid with fibres grouped in a layer across the propagation direction X

4.4. Analyses using a two-dimensional representative rectangular cell

The (non-uniform) fibrous representation in the form of cuboid *RVE-2* was developed in a rather uneconomic way and the volume element tends to be relatively large and it contains many relatively-long straight fragments of fibres. Therefore, a question arises whether a simpler volume element (i.e., with less fibres) can provide results with at least similarly good agreement to the measurements. It seems to be fairly possible, and in fact, it means that some optimized locally-representative arrangement of fibres should be sought. As a matter of fact, the necessity to carry on some optimizing trials, which are computationally demanding in 3D, leads to another question, namely: is it possible to find a two-dimensional representation which may be – to some satisfactory degree – equivalent to three-dimensional representations? In fact, two-dimensional representations of compact and open fluid domains found in fibrous materials can be constructed as arrangements of fibre cross-sections set in a two-dimensional cell, however, formally, they would represent *exactly* only specific materials which have all straight fibres in parallel and across the direction of propagation. Therefore, in the two-dimensional case one should rather speak about *quasi* representativeness.

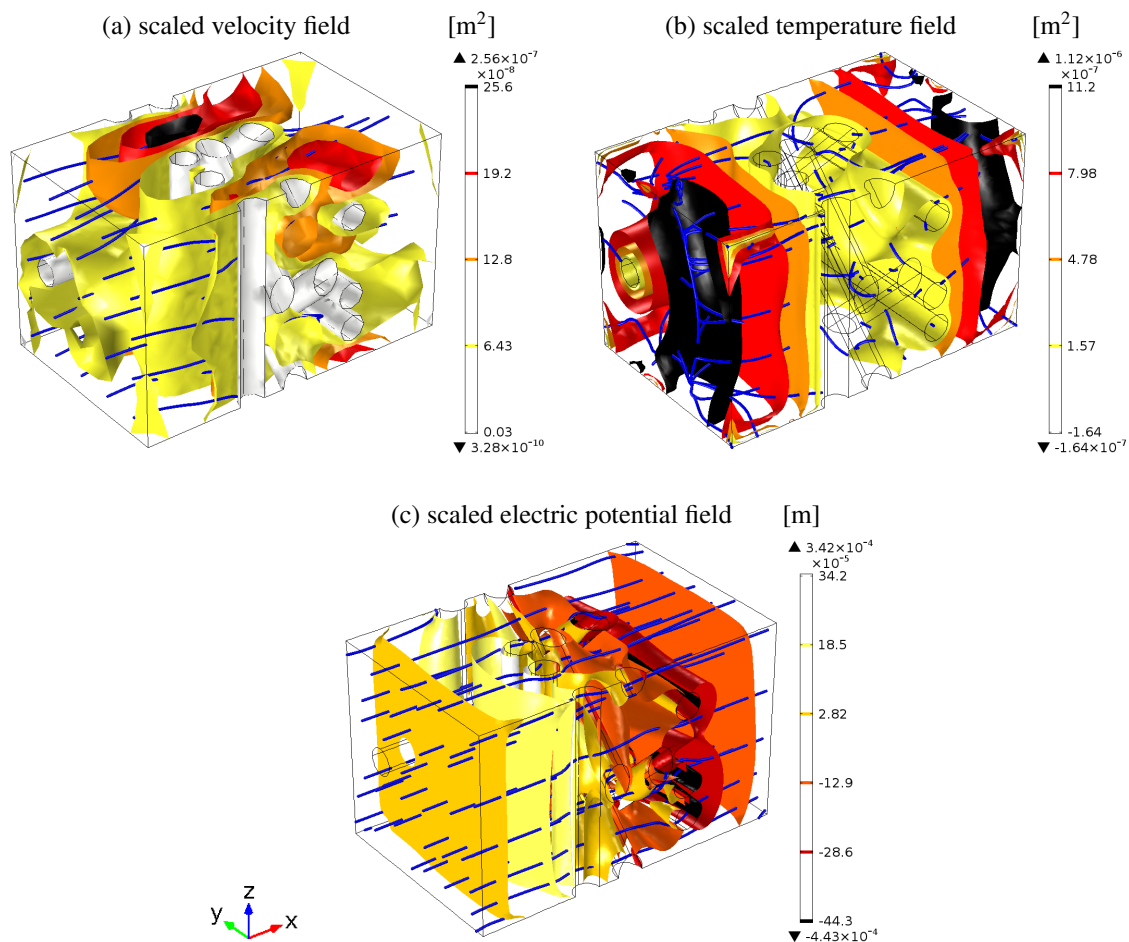
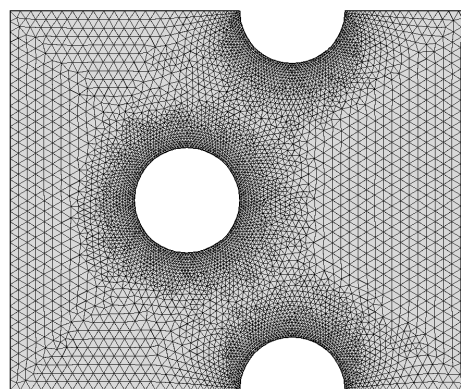


Figure 8: Solutions of microstructural problems in the fluid domain of the cuboid fibrous representation *RVE-2*

On the other hand, even three-dimensional representations are only statistically-equivalent periodic realizations of a typical local geometry (which in reality, slightly varies in a whole fibrous medium and is *not* periodic). Anyway, it is always the case of capturing important features of the microstructure geometry which are crucial for the overall macroscopic wave propagation and damping.

A few concepts of a two-dimensional *quasi*-representative cell were tested (involving also elliptic cross-sections to simulate slanted fibres), however, a very simple case will be presented here since already that one provided astonishingly good results. The two-dimensional cell has a rectangular shape – it is longer in the direction of wave propagation. It has porosity of 90% and contains only two fibres (i.e., two complete circular fibre cross-sections) set up rather closely in order to form an efficient



→ X – the direction of propagation

Figure 9: Two-dimensional representation *Cell-2D* of fibrous material with porosity 90%, in the form of a periodic rectangular cell with two (complete) fibres

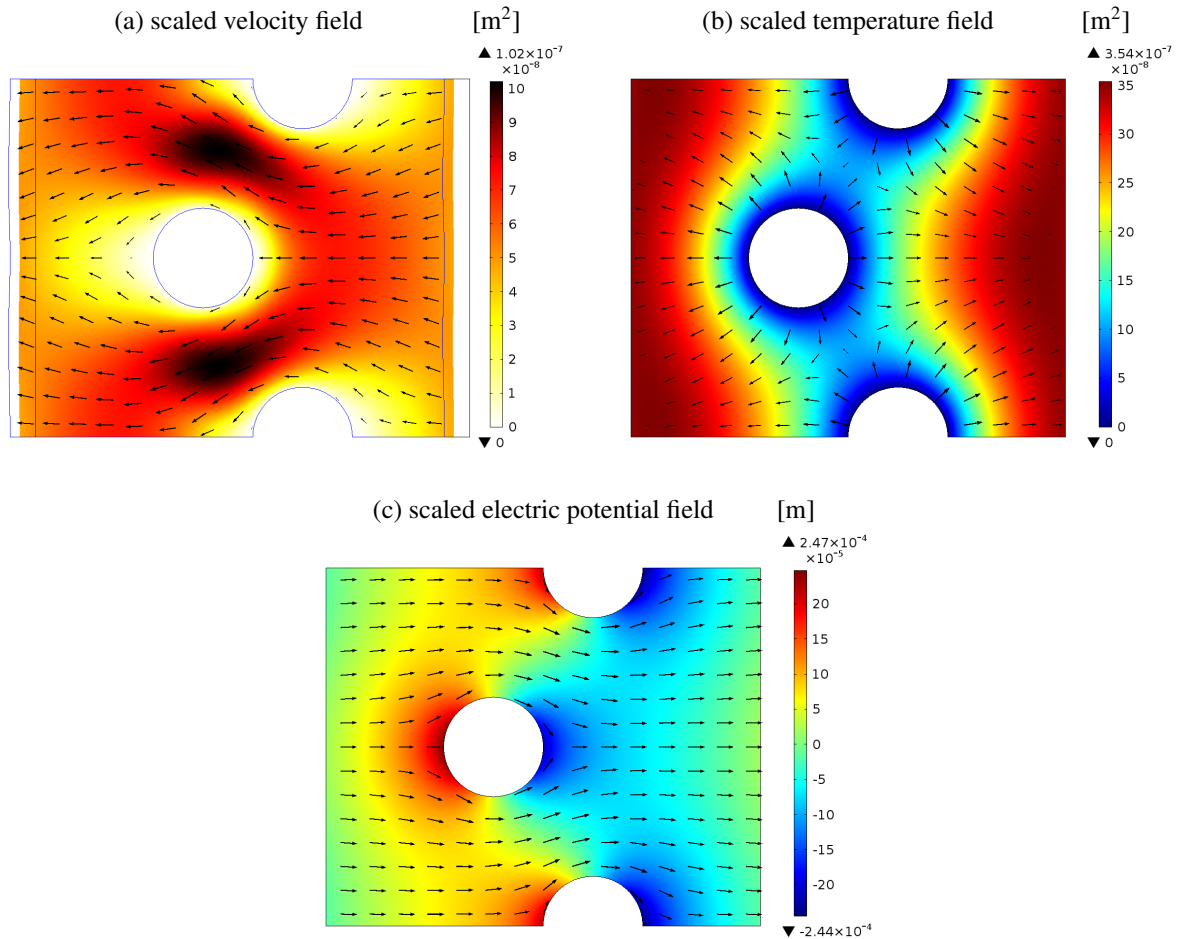


Figure 10: Solutions of microstructural problems in the fluid domain of the two-dimensional fibrous representation *Cell-2D*

fibre layer perpendicular to the direction of propagation (see Figure 9). In that way it is based on the assumption tested already in the cuboid volume element. The size of two-dimensional cell was set so that the diameter of fibre cross-sections was 0.5 mm, and the proportions of rectangle were optimized in order to get a better resemblance between the calculated acoustic absorption curves and the experimental ones measured for wire samples. This is some kind of a fit on the data and the link between microstructure and the macroscopic acoustical behaviour is somewhat lost. Moreover, the fibre concentration fit in this simplified *quasi*-representative two-dimensional cell (where all fibres are in parallel) is somehow different from the fit in the three-dimensional RVE-2. Figure 9 shows the final representative cell (*Cell-2D*) with the finite element mesh which was used in the micro-structural finite element analyses; the obtained solutions – in the form of scaled fields – are shown in Figure 10. The corresponding values of transport parameters are listed for *Cell-2D* in Table 1 and the results of calculations based on them are discussed in Section 4.5.

4.5. Results of the multiscale modelling

The transport parameters calculated from various periodic representations of fibrous microstructure served to calculate the dynamic tortuosity functions, $\alpha(\omega)$ and $\alpha'(\omega)$, and then, the functions of effective density, $\rho_e(\omega)$, and bulk modulus, $K_e(\omega)$ using formulas (1); all this allowed to determine the effective speed of sound which is also a complex and frequency-dependent function:

$$c_e(\omega) = \sqrt{\frac{K_e(\omega)}{\rho_e(\omega)}} = \frac{c_f}{\sqrt{\alpha(\omega)\beta(\omega)}}, \quad (2)$$

where $c_f = \sqrt{K_f/\rho_f}$ is the speed of sound in pore-fluid (air). Now, the effective speed of sound can be used to calculate the complex wavenumber in the following standard way:

$$k_w(\omega) = \frac{\omega}{c_e(\omega)} = \frac{\omega}{c_f} \sqrt{\alpha(\omega)\beta(\omega)}. \quad (3)$$

The imaginary part of this frequency-dependent function is always negative (for $\omega > 0$, and assuming that the convention $+i\omega t$ has been used for the time-harmonic *ansatz*, where i is the imaginary unit and t denotes time), and thus, the complex wavenumber

may be decomposed into its real and imaginary parts as follows: $k_w(\omega) = \text{Re } k_w(\omega) + i \text{Im } k_w(\omega) = \omega/c_w(\omega) - i d_w(\omega)$, where:

$$c_w(\omega) = \frac{\omega}{\text{Re } k_w(\omega)}, \quad d_w(\omega) = -\text{Im } k_w(\omega) \quad (4)$$

are the real-valued (and positive for $\omega > 0$) frequency-dependent functions of wave speed and damping, respectively. (Notice that $c_w = c_f / \text{Re}[\sqrt{\alpha\beta}]$ is not the same as $\text{Re } c_e = c_f \text{Re}[1/\sqrt{\alpha\beta}]$.) These functions were calculated for three considered microstructure representations discussed above, namely: *RVE-1* – the cubic volume element, *RVE-2* – the elongated cuboid volume element, and *Cell-2D* – the rectangular two-dimensional cell. The results are presented in Figure 11 for the wave speed, and in Figure 12 for the wave damping. The acoustic wave speed in air-saturated fibrous media is always slower than the speed of sound in the air c_f , however, for the considered fibrous material with very thick and loosely set fibres, it is more than $0.9c_f$ for frequencies higher than 1 kHz, and still more than $0.85c_f$ for frequencies higher than 100 Hz; the acoustic waves below 100 Hz slow down dramatically. It is noticeable that the wave speeds calculated for the representations *RVE-2* and *Cell-2D* are almost identical in nearly the whole frequency range, already above 40 Hz, and they slightly though distinctly differ from the result calculated for *RVE-1*. Also the wave damping calculations are similar for *RVE-2* and *Cell-2D* at least above 500 Hz; one

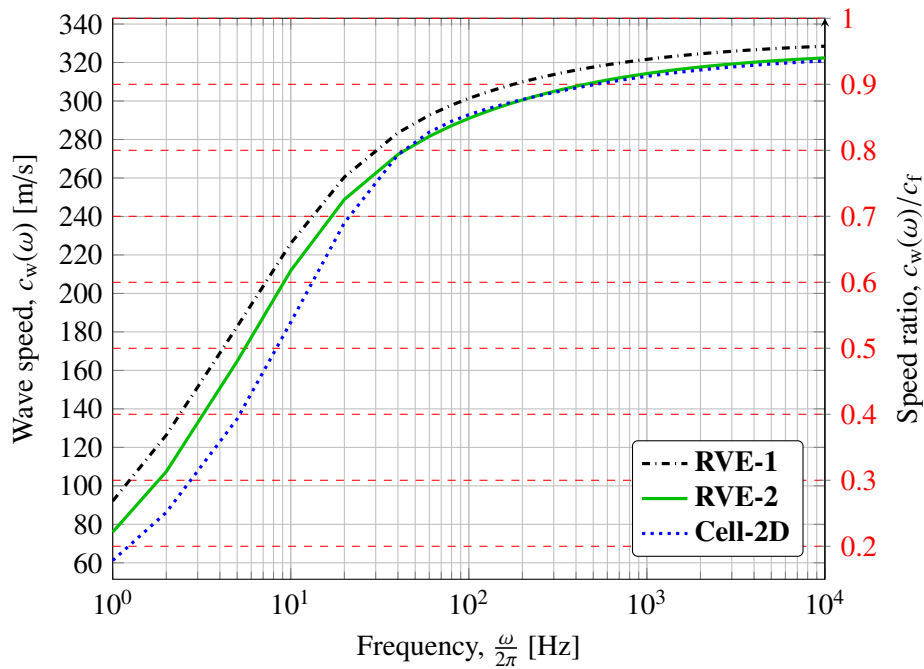


Figure 11: Acoustic wave speed (and its ratio to the speed of sound in the air) in the air-saturated fibrous material with porosity 90%, computed from three different representations of its microstructure

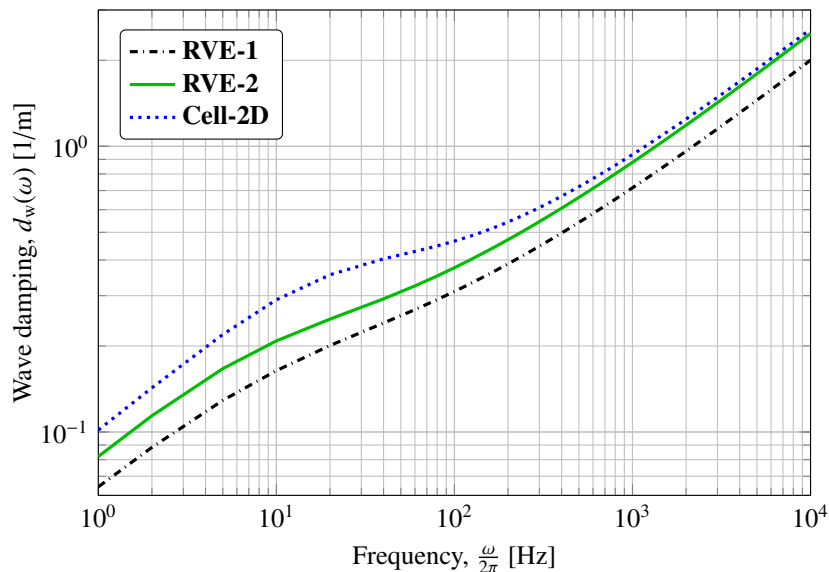


Figure 12: Wave damping in the fibrous material with porosity 90%, computed from three different representations of its microstructure

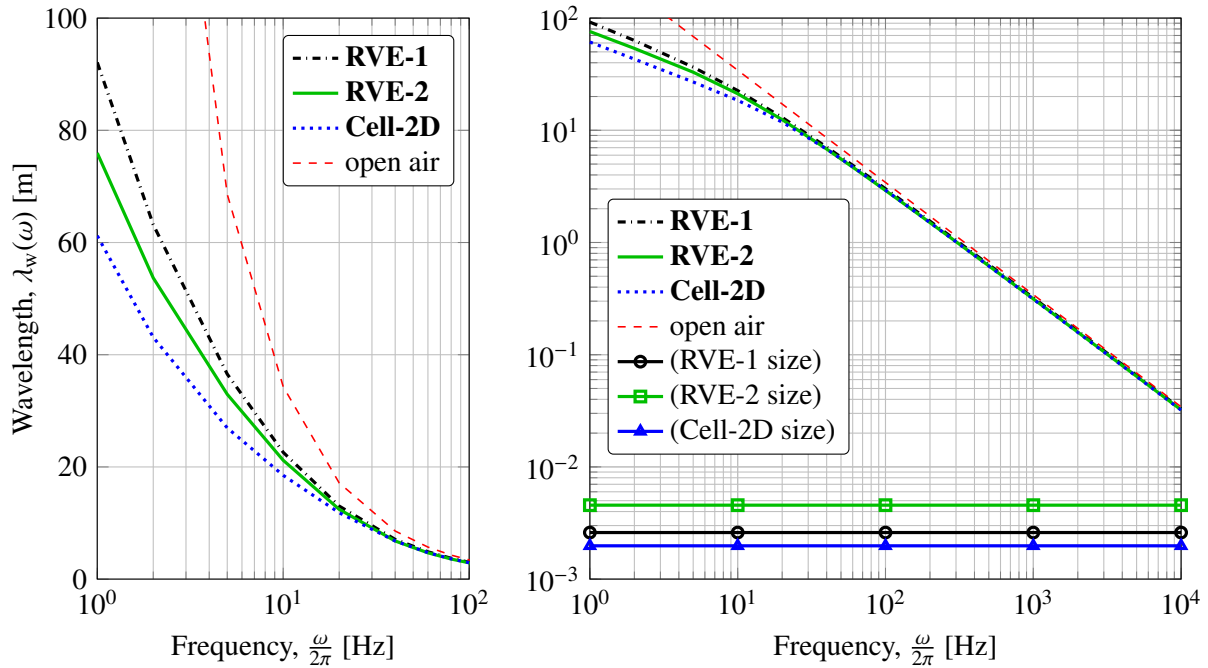


Figure 13: Wavelength in the fibrous material with porosity 90%, computed from three different representations of its microstructure (and compared with the wavelength of sound in the open air)

should notice that the logarithmic scale is used in Figure 12 to plot these characteristics. The wave damping computed from the representation *RVE-1* is significantly lower. These observations of similarities will be somehow confirmed below by the calculations of sound absorption.

Figure 13 presents the wavelengths computed for the proposed representations of fibrous material: large differences between the results can be observed *only* at extremely low frequencies. It is important to observe that for all representations the wavelength at 6.4 kHz (the highest measurement frequency) is about 50 mm, which is 25 times larger than 2.0 mm – the size of *Cell-2D*, and about 19 times larger than 2.6 mm – the size of *RVE-1*, and only 11 times larger than 4.5 mm – the size of *RVE-2*. This raises a question about the scale separation at higher frequencies. The issue will be discussed further (in Sections 5 and 6), after presenting the results for a fibrous material braided from oblate wire (see also a discussion on the matter in [53]).

The real-valued frequency-dependent acoustic absorption coefficient is calculated as follows [1]

$$A(\omega) = 1 - |R(\omega)|^2, \quad R(\omega) = \frac{Z(\omega) - Z_f}{Z(\omega) + Z_f} \quad (5)$$

where $Z_f = \rho_f c_f$ is the characteristic impedance of pore-fluid (air), and

$$Z(\omega) = -i \rho_e(\omega) c_e(\omega) \cot \left[\frac{\omega h}{c_e(\omega)} \right] = -i \frac{Z_f}{\phi} \sqrt{\frac{\alpha(\omega)}{\beta(\omega)}} \cot \left[\frac{\omega h}{c_f} \sqrt{\alpha(\omega) \beta(\omega)} \right] \quad (6)$$

is the complex frequency-dependent surface acoustic impedance of a sound absorbing layer of porous (fibrous) material with open porosity ϕ and thickness h , set on the rigid wall. It was found by analytically solving the relevant Helmholtz problem of a layer of equivalent fluid – with thickness h , the density $\rho_e(\omega)$, and the speed of sound $c_e(\omega)$ – set to the rigid wall and subject on its free surface to a normal plane incident harmonic wave.

Figure 14 shows the acoustic absorption coefficient computed for fibrous layers with thickness (height) $h = 30$ mm, 60 mm, and 90 mm, for each of the considered representations: *RVE-1*, *RVE-2*, and *Cell-2D*. The microstructure-based calculations are also compared with some corresponding experimental curves measured for the copper-wire samples. The results of sound absorption obtained from the cubic volume element *RVE-1*, with fibres placed uniformly, are systematically underestimated with respect to the measurements (see Figure 14). On the other hand, for each case of layer thickness, the character of the corresponding numerical and experimental curves is in fact the same, which suggested only some modifications to the representative geometry, based on some additional observations of wire samples. In fact, in real samples a fibre concentration is observed and this feature must be somehow introduced in order to keep a link with the actual microstructure. This was achieved by grouping fibres into a denser layer in the cuboid *RVE-2*; the same concept was also applied in the *quasi*-representative rectangular *Cell-2D*. Both representations provided almost identical curves of the wave speed and damping as well as the acoustic absorption curves, which suggests some 3D-2D representative equivalence for the studied fibrous material, that is, the features most crucial for sound absorption can be captured using two-dimensional representations (as the one proposed in this paper) of the essentially three-dimensional arrangement of fibrous medium. The sound absorption calculated for each layer is now on the same level

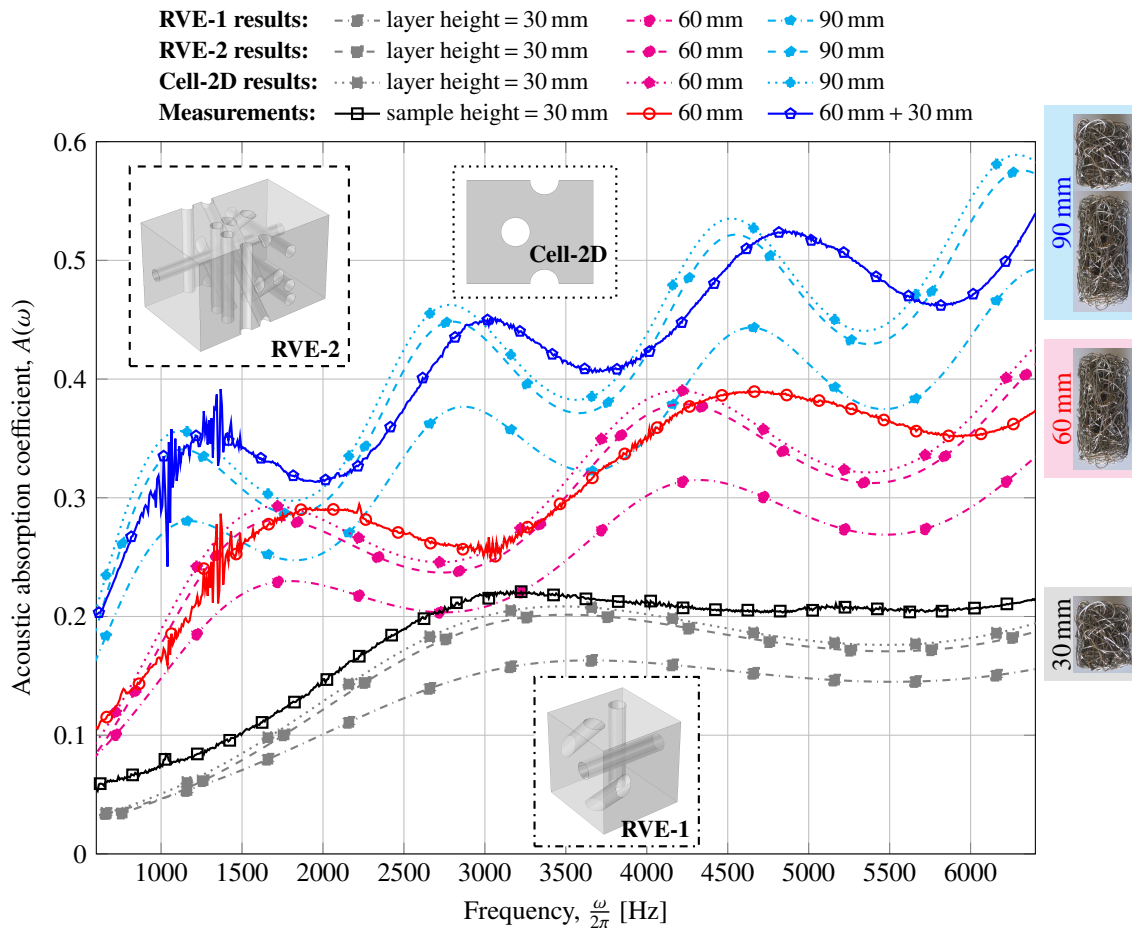


Figure 14: Acoustic absorption of fibrous material with porosity 90%, fibre diameter 0.5 mm, and various thickness (i.e., the layer height), computed from three different representations of fibrous microstructure, and compared with the corresponding experimental results measured for the copper-wire samples

as the results measured for the corresponding wire samples (see Figure 14). The discrepancies are acceptable, although one may observe a systematic shift in the maxima/minima of the computed absorption to slightly lower frequencies than the ones manifested in the experimental results. A similar though a bit smaller shift is also observable in the *RVE-1* calculations for which the wave propagation is faster (see Figure 11). Undoubtedly, a dense layer of fibres in *RVE-2* (or *Cell-2D*) slows down the waves penetrating fibrous microstructures. However, the proposed arrangement of straight fibres in a volume element may still be improved to allow for a little bit higher wave speeds with possibly the same level of damping.

5. Results for oblate wire

Numerical estimations and yet another experimental validation were performed in order to verify the correctness of the proposed computationally economical approach based on *quasi*-representative two-dimensional cells for fibrous media.

Firstly, numerical estimations were done for a possible fibrous material from oblate wire. It was assumed that the oblate wire would be obtained by flattening the round (copper) wire with diameter $D = 0.5$ mm, so that its cross section is no longer circular but oblate with some assumed height H (i.e., flat wire thickness, see Figure 15) and appropriately enlarged width. The overall cross-sectional area of oblate wire was assumed similar to the original round wire. For the micro-scale computations two-dimensional periodic cells with two fibres were used. The porosity of cells is 90% and their proportions and fibre distribution inside the rectangular fluid domain are the same as in the two-dimensional cell proposed beforehand for round wire (see Figures 9 and 15). A new factor is an orientation of the oblate cross-section inside 2D cell: an average position was assumed, namely, oblate fibres are aslant with respect to the direction of propagation (and mutually skewed), that is, they are not parallel nor perpendicular to each other nor to the horizontal direction inside the rectangular cell (see Figure 15). The transport parameters were computed for a few cases of such *quasi*-representative cells, and the results are given in Table 2 for: (a) the circular cross-section (i.e., of round wire) with diameter $D = 0.5$ mm, (b) an oblate cross-section with height $H = 0.3$ mm, and (c) an oblate cross-section with height $H = 0.2$ mm. These parameters were used in macro-scale calculations of the acoustic absorption of fibrous layers with thickness of 90 mm. Figure 15 presents the sound absorption curves computed in the wide frequency range (up to 8.5 kHz). One should observe a very small difference between the sound absorption of the fibrous layer of round wire with diameter $D = 0.5$ mm and the layer of oblate wire with the cross-section flattened to $H = 0.3$ mm. On the other hand, when the wire is

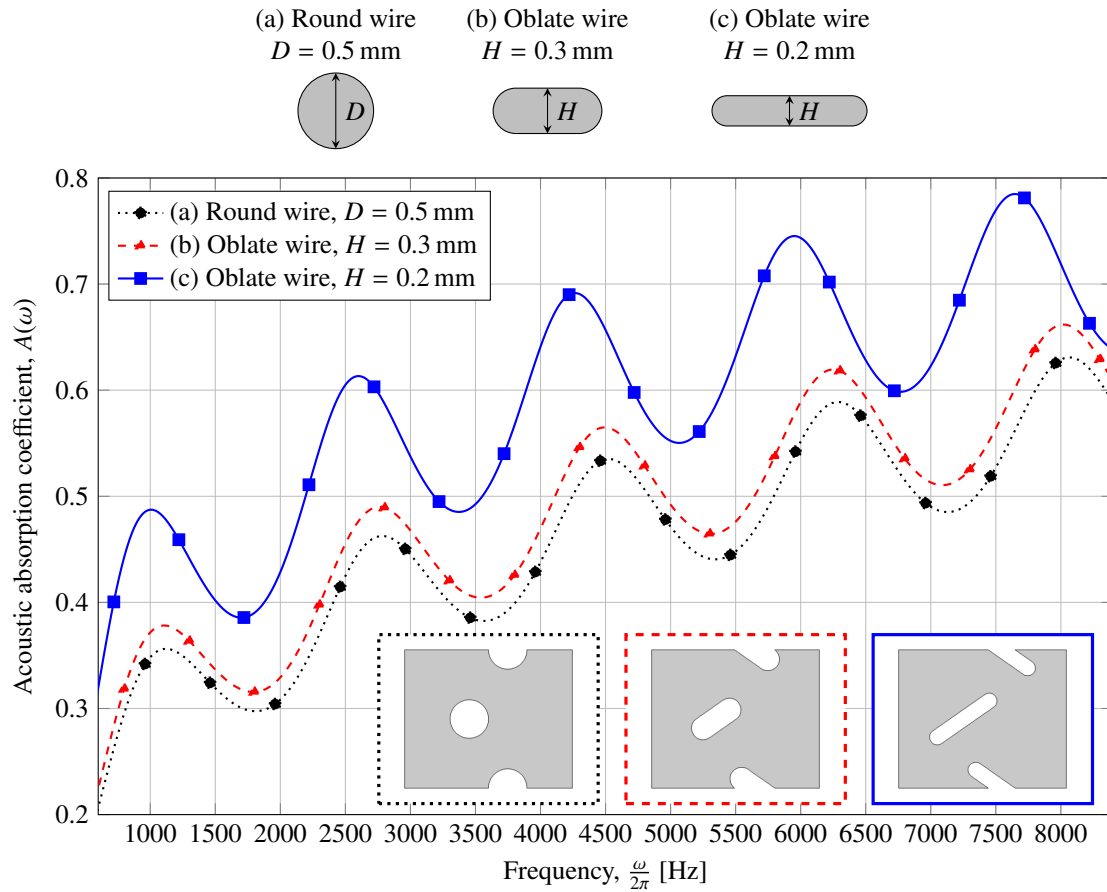


Figure 15: Sound absorption calculated for 90 mm-thick fibrous layers of wire with round or oblate cross-section – numerical estimations were based on the *quasi* representative two-dimensional periodic cells with porosity 90%

Table 2: Transport parameters (for JCAPL model) computed from 2D cells *quasi* representative for fibrous materials with porosity 90%, manufactured from round wire with diameter $D = 0.5$ mm (D:0.5), or from oblate wire with cross-section height $H = 0.3$ mm (H:0.3), or $H = 0.2$ mm (H:0.2); additionally, 5 transport parameters determined by inverse characterisations based on JCAL model and using the curves of surface acoustic impedance measured for the round wire samples D:0.5, and for the oblate wire samples H:0.2

Parameter	Unit	Microstructure-based calculations of parameters for JCAPL model			Inverse identification: JCAL model	
		D:0.5	H:0.3	H:0.2	D:0.5	H:0.2
viscous permeability, k_0 :	$[10^{-9} \text{m}^2]$	48.7	44.7	27.5	40.1	22.5
thermal permeability, k'_0 :	$[10^{-9} \text{m}^2]$	204	182	142	192	56.0
(inertial) tortuosity, α_∞ :	[-]	1.12	1.12	1.22	1.10	1.16
viscous static tortuosity, α_0 :	[-]	1.30	1.32	1.46	—	—
thermal static tortuosity, α'_0 :	[-]	1.20	1.22	1.26	—	—
viscous charact. length, Λ :	[mm]	1.08	1.01	0.77	1.03	0.70
thermal charact. length, Λ' :	[mm]	2.25	1.99	1.55	1.81	1.61

more flattened, so that the height of cross-section is reduced to $H = 0.2$ mm (and its width is appropriately enlarged), then, the sound absorption is significantly increased in the whole frequency range. In fact, this observation was decisive when preparing wire for new fibrous samples for experimental validations.

The round copper wire with diameter $D = 0.5$ mm was flattened so that its thickness was reduced to $H = 0.2$ mm (and the cross-section width enlarged to nearly 0.9 mm). In the process, the length of wire pieces was also increased – from the original 10 cm to more than 11 cm – see Figure 16. Such flattened pieces of oblate wire were used to manufacture two fibrous samples (see Figure 16) in the manner identical with the one described in Section 2. The sample dimensions are as in the case of round wire samples, namely, the diameter is 29 mm and their heights are 30 mm and 60 mm, so that their porosity is 90%, since, respectively, 10 m and 20 m of the original copper wire were used to manufacture them. The samples were measured in the impedance tube (see Figure 16): small and large sample separately, and in pairs with the total thickness of 90 mm (i.e., 30 mm + 60 mm and 60 mm + 30 mm). The results of sound absorption shown in Figure 17 prove to be in a very good agreement with the corresponding numerical estimations based on the two-dimensional *quasi*-representative cell. Moreover, perhaps the



Figure 16: A piece of oblate wire (with its rounded original below) and two fibrous samples with porosity 90% (one of the samples is shown also inside the impedance tube)

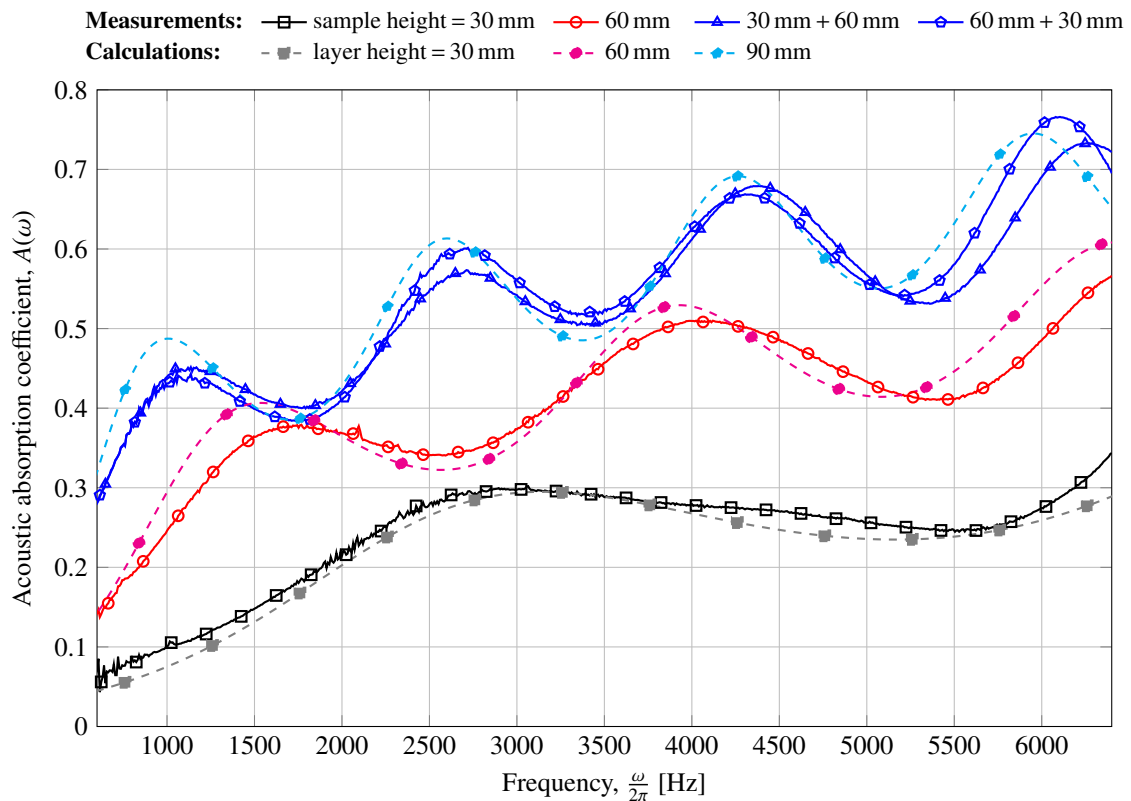


Figure 17: Sound absorption measured in the impedance tube for the fibrous samples (with porosity 90%) manufactured from the oblate copper wire (with cross-sectional thickness 0.2 mm), and the corresponding numerical estimations

quasi-representative cell could be improved: the size and rectangle can be but slightly modified when the width of cross-section is slightly reduced (as in reality) to account for the enlarged length of the flattened wire. The small discrepancies may be neglected; in fact, they ensue from some geometrical deviations of oblate wire and overall imperfections of samples, and also from a poorer separation of scales at higher frequencies as suggested by the following results concerning wavelengths and surface acoustic impedance.

Figure 18 shows wavelengths computed in the frequency range up to 10 kHz. For example, the wavelength is 64 mm at 5 kHz, and 54 mm at 6 kHz, which is, respectively, 32 or 27 times larger than 2 mm – the size of representative cell used for these calculations. Figure 19 compares the surface acoustic impedance computed for the fibrous layer 90 mm thick, and measured in

the impedance tube with two fibrous samples inside. (In fact, these results served to determine the acoustic absorption coefficient as shown by formulas (5).) Here, the agreement or discrepancies between numerical calculations and measurements can be observed separately for the real and imaginary parts. One may notice that the largest discrepancy between the calculations and measurements are at higher frequencies, above 5 kHz, which can be related to a worse separation of scales, but also some smaller

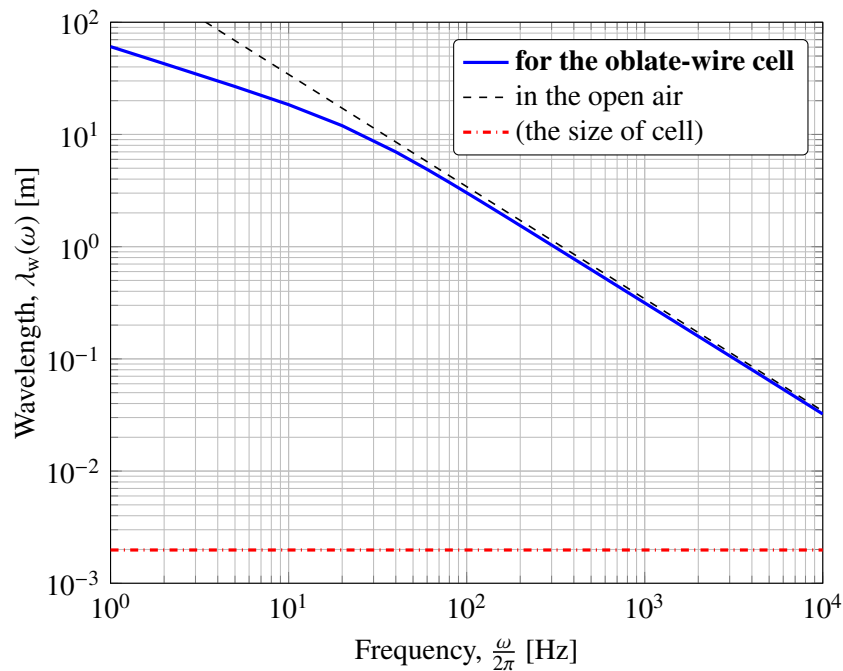


Figure 18: Wavelengths computed for the material with oblate fibres and porosity 90% (and compared with the wavelength of sound in the open air and the size of representative cell used in calculations)

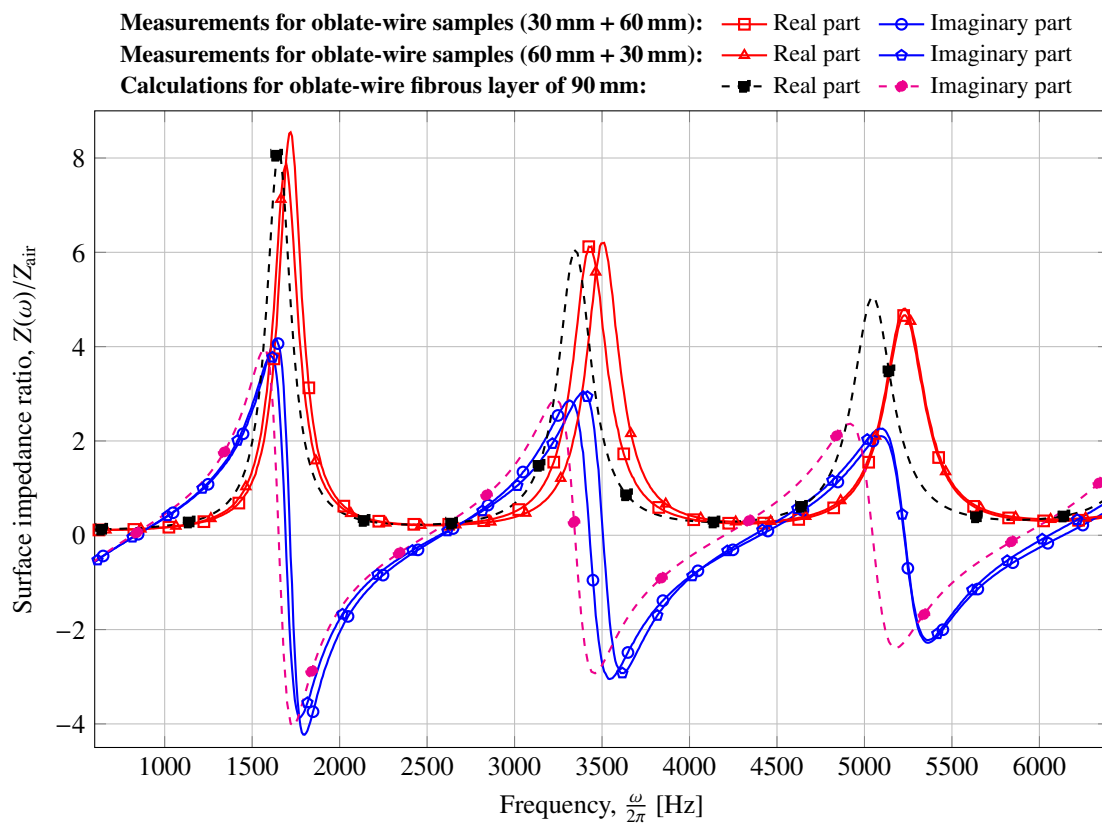


Figure 19: Surface acoustic impedance (the real and imaginary parts) measured for 90 mm thick layers of two fibrous samples made up from oblate wire and put together into the impedance tube; the experimental results are compared with the corresponding numerical calculations based on the two-dimensional representative cell

scale imperfections in fibrous samples not present in the periodic representation. The measured curves of surface acoustic impedance were also used by a normalised inverse characterisation method [54] to characterise the parameters of the fibrous material from oblate wire with respect to the Johnson-Champoux-Allard-Lafarge (JCAL) model [1, 6]. In this model the *static* viscous and thermal tortuosities are *not used*, and moreover, the inverse characterisation procedure was fed only with single-layer measurements (i.e., without air cavities), therefore, the discovered values must be treated as approximative, though they are similar to the parameters calculated from microstructure. An inverse characterisation was also carried out for the round wire material using the JCAL model. The five transport parameters identified for both materials using the inverse method based on the JCAL model are listed in two separate columns in Table 2.

6. Conclusions

The non-uniform arrangement of fibres were found to be representative for the fibrous samples manufactured of copper wire. Different 3D and 2D non-uniform representations were proposed since the fibre concentration parameter is fitted and the direct link between the microstructure and the macroscopic acoustical behaviour may be somewhat lost. The microstructure-based calculations showed that (for the same porosity, fibre thickness and shape) such non-uniform arrangements ensure more damping, although at the same time, perhaps the waves propagate a little bit faster in the investigated copper-wire samples. Nevertheless, the discrepancies are acceptable and it seems that they are rather caused by the strained periodicity of arrangements used in modelling, and not by a misconception in the assumption of straight fibres, that is, if not the constraint of periodicity, a better representation with straight fibres could be easily constructed.

The arrangement of fibres in manually braided wire samples was rather complex and certainly three-dimensional, therefore, the demonstrated agreement between 2D and 3D representations shows some potential in use of 2D cells *quasi*-representative for fibrous media, as pointed out below.

In the cuboid volume elements (and rectangular 2D cells) fibres are grouped in layers which perhaps entails some sort of anisotropy at the macro-scale level. In fact, one may expect some kind of transversal isotropy with the isotropy planes normal to the direction of propagation. It means that the transport properties, like permeability and tortuosity, determined along this direction can be substantially different from the values found for the direction across to it (see, for example, measurements of anisotropic air flow resistivity by Tarnow [55] for a glass wool). Nevertheless, the considered configuration and problem of plane wave propagation allow for the investigations based on the assumption of macroscopic homogeneity and isotropy with the transport parameters computed for the flow/conductivity along the direction of propagation. It seems that anisotropic effects should be taken into account in case of truly anisotropic *poroelastic* materials [56–60], where the vibration of elastic skeleton (fibres) cannot be neglected, and the anisotropy strongly affects their elastic behaviour and also visco-thermal dissipations.

The discussed analyses and microstructure-based approach involving the JCAPL model can be used to develop a simple three-parameter model for sound absorbing fibrous media, which would employ a few direct geometric features, namely, the porosity, the (average) thickness of fibres, and the ratio of the density of fibre distribution along the direction of wave propagation to the density of distribution crosswise, or an equivalent parameter describing some similar anisotropy in fibre arrangement. As a matter of fact, this new parameter should somehow describe the concentration of fibres which is related to the throat size which controls the viscous permeability [17] – a very important parameter for overall sound propagation and absorption. If well constructed, such a model should be more versatile than many of simple yet very restricted phenomenological models of fibrous materials, and at the same time it would be much simpler, straightforward and “user-friendly” than the underlying 8-parameter JCAPL model.

Some variations of fibrous microstructure geometry can be analysed using two-dimensional representations provided that the assumptions of sufficiently long and locally straight fibres are fulfilled (which is in fact, the case of many fibrous materials). It seems that two-dimensional cells can be successfully used to represent many sound absorbing fibrous media in the case of numerical investigations on the effects of various thickness of fibres, different shape of fibre cross-sections, and the relative density of fibre distribution along the propagation direction and across to it. This observation is essentially confirmed with the presented results of numerical and experimental study of fibrous layers made up from oblate wire.

Although the simplest from the proposed periodic representations contain only a few fibres and so the periodic cell size is only about 2 mm, the effect of a worse separation of scales seems to be obvious at higher frequencies. However, there are perhaps two main reasons for larger discrepancies at higher frequencies: (1) the obvious poorer separation of scales, (2) small imperfections in real fibrous samples which are not present in the simplified idealised micro-geometric representations but relevant for higher frequency effects, for example, oblate wire roughness and sharpness at edges and endings, etc. On the other hand, it seems that a worse separation of scales (of the order less than 10^2) causes only a gradual deterioration of results and the method does not fail. As a matter of fact, the general idealisations which contradict the irregularities in real fibrous samples (the real material is *not* periodic, the fibres are *not* straight everywhere, etc.) tend to be more important in the whole frequency range.

The effect of fibres’ endings is missing, however, this can be included in volume elements. The question remains, however, how short the real fibres must be to necessitate such approach. Moreover, the number of fibres’ endings per volume of fibrous medium must also be observed and a *single* isolated fibre tip in a *periodic* volume element is possible only in the case of locally-curved fibres. On the other hand, adding curved and, especially, truncated fibres to a volume element is less restricted by the requirement of periodicity than in the case of straight obliquely passing-through fibres studied in the present work.

Acknowledgements

Financial support of the Project “Relations between the micro-geometry and sound propagation and absorption in porous and poroelastic media”, No. 2015/19/B/ST8/03979, financed by the Polish National Science Centre (NCN), is gratefully acknowledged. Dissemination of this work was also supported by COST (European Cooperation in Science and Technology) through the COST Action CA15125 – DENORMS: “Designs for Noise Reducing Materials and Structures”.

References

- [1] J. F. Allard, N. Atalla, *Propagation of Sound in Porous Media: Modelling Sound Absorbing Materials*, Second Edition, Wiley, 2009.
- [2] D. L. Johnson, J. Koplik, R. Dashen, Theory of dynamic permeability and tortuosity in fluid-saturated porous media, *J. Fluid Mech.* 176 (1987) 379–402.
- [3] Y. Champoux, J.-F. Allard, Dynamic tortuosity and bulk modulus in air-saturated porous media, *J. Appl. Phys.* 70 (1991) 1975–1979.
- [4] S. R. Pride, F. D. Morgan, A. F. Gangi, Drag forces of porous-medium acoustics, *Phys. Rev. B* 47 (1993) 4964–4978.
- [5] D. Lafarge, *Propagation du son dans les matériaux poreux à structure rigide saturés par un fluide viscothermique* [Sound propagation in porous materials with rigid frame saturated by a viscothermal fluid], PhD thesis, Université du Maine (France), 1993.
- [6] D. Lafarge, P. Lemarinier, J. F. Allard, V. Tarnow, Dynamic compressibility of air in porous structures at audible frequencies, *J. Acoust. Soc. Am.* 102 (1997) 1995–2006.
- [7] D. Lafarge, The equivalent fluid model, Chapter 6 (pp. 167–201) in: *Materials and Acoustics Handbook*. ISTE – Wiley, 2009.
- [8] M. E. Delany, E. N. Bazley, Acoustical properties of fibrous absorbent materials, *Appl. Acoust.* 3 (1970) 105–116.
- [9] Y. Miki, Acoustical properties of porous materials – Modifications of Delany-Bazley models, *J. Acoust. Soc. Jpn.* 11 (1990) 19–24.
- [10] Y. Miki, Acoustical properties of porous materials – Generalizations of empirical models, *J. Acoust. Soc. Jpn.* 11 (1990) 25–28.
- [11] N. Voronina, Improved empirical model of sound propagation through a fibrous material, *Appl. Acoust.* 48 (1996) 121–132.
- [12] T. G. Zieliński, Numerical investigation of active porous composites with enhanced acoustic absorption, *J. Sound Vib.* 330 (2011) 5292–5308.
- [13] C. Perrot, R. Panneton, X. Olny, Periodic unit cell reconstruction of porous media: Application to open-cell aluminum foams, *J. Appl. Phys.* 101 (2007) 113538.
- [14] C. Perrot, F. Chevillotte, R. Panneton, Dynamic viscous permeability of an open-cell aluminum foam: Computations versus experiments, *J. Appl. Phys.* 103 (2008) 024909.
- [15] F. Chevillotte, C. Perrot, R. Panneton, Microstructure based model for sound absorption predictions of perforated closed-cell metallic foams, *J. Acoust. Soc. Am.* 128 (2010) 1766–1776.
- [16] C. Perrot, F. Chevillotte, M. T. Hoang, G. Bonnet, F.-X. Bécot, L. Gautron, A. Duval, Microstructure, transport, and acoustic properties of open-cell foam samples: experiments and three-dimensional numerical simulations, *J. Appl. Phys.* 111 (2012) 014911.
- [17] C. Perrot, F. Chevillotte, R. Panneton, Bottom-up approach for microstructure optimization of sound absorbing materials, *J. Acoust. Soc. Am.* 124 (2008) 940–948.
- [18] T. G. Zieliński, Inverse identification and microscopic estimation of parameters for models of sound absorption in porous ceramics, in: P. Sas, D. Moens, S. Jonckheere (Eds.), *Proceedings of International Conference on Noise and Vibration Engineering (ISMA2012) / International Conference on Uncertainty in Structural Dynamics (USD2012)*, 2012, pp. 95–108.
- [19] T. G. Zieliński, Generation of random microstructures and prediction of sound velocity and absorption for open foams with spherical pores, *J. Acoust. Soc. Am.* 137 (2015) 1790–1801.
- [20] J. H. Park, S. H. Yang, H. R. Lee, C. B. Yu, S. Y. Pak, C. S. Oh, Y. J. Kang, J. R. Youn, Optimization of low frequency sound absorption by cell size control and multiscale poroacoustics modeling, *J. Sound Vib.* 397 (2011) 17–30.
- [21] S. Gasser, F. Paun, Y. Bréchet, Absorptive properties of rigid porous media: Application to face centered cubic sphere packing, *J. Acoust. Soc. Am.* 117 (2005) 2090–2099.
- [22] C.-Y. Lee, M. J. Leamy, J. H. Nadler, Acoustic absorption calculation in irreducible porous media: A unified computational approach, *J. Acoust. Soc. Am.* 126 (2009) 1862–1870.
- [23] T. G. Zieliński, Microstructure-based calculations and experimental results for sound absorbing porous layers of randomly packed rigid spherical beads, *J. Appl. Phys.* 116 (2014) 034905.
- [24] R. Venegas, O. Umnova, Acoustical properties of double porosity granular materials, *J. Acoust. Soc. Am.* 130 (2011) 2765–2776.
- [25] F. Chevillotte, C. Perrot, E. Guillon, A direct link between microstructure and acoustical macro-behavior of real double porosity foams, *J. Acoust. Soc. Am.* 134 (2013) 4681–4690.
- [26] I. Malinuskaya, V. V. Mourzenko, J.-F. Thovert, P. M. Adler, Wave propagation through saturated porous media, *Phys. Rev. E* 77 (2008) 066302.
- [27] T. Yamamoto, S. Maruyama, K. Terada, K. Izui, S. Nishiwaki, A generalized macroscopic model for sound-absorbing poroelastic media using the homogenization method, *Comput. Methods Appl. Mech. Engrg.* 200 (2011) 251–264.
- [28] M. T. Hoang, G. Bonnet, H. T. Luu, C. Perrot, Linear elastic properties derivation from microstructures representative of transport parameters, *J. Acoust. Soc. Am.* 135 (2014) 3172–3185.
- [29] K. Gao, J. van Dommelen, P. Göransson, M. G. D. Geers, A homogenization approach for characterization of the fluid-solid coupling parameters in Biot’s equations for acoustic poroelastic materials, *J. Sound Vib.* 351 (2015) 251–267.
- [30] T. G. Zieliński, On representativeness of the representative cells for the microstructure-based predictions of sound absorption in fibrous and porous media, in: *Proceedings of EuroNoise 2015 – the 10th European Congress and Exposition on Noise Control Engineering*, 2015, pp. 2473–2478.
- [31] A. Cortis, J. G. Berryman, Frequency-dependent viscous flow in channels with fractal rough surfaces, *Phys. Fluids* 22 (2010) 053603.
- [32] H. V. Tafreshi, M. S. A. Rahman, S. Jaganathan, Q. Wang, B. Pourdeyhimi, Analytical expressions for predicting permeability of bimodal fibrous porous media, *Chem. Eng. Sci.* 64 (2009) 1154–1159.
- [33] P.-C. Gervais, N. Bardin-Monnier, D. Thomas, Permeability modelling of fibrous media with bimodal fibre size distribution, *Chem. Eng. Sci.* 73 (2012) 239–248.

- [34] K. Yazdchi, S. Srivastava, S. Luding, Microstructural effects on the permeability of periodic fibrous porous media, *Int. J. Multiphase Flow* 37 (2011) 956–966.
- [35] S. Jaganathan, H. V. Tafreshi, B. Pourdeyhimi, A realistic approach for modelling permeability of fibrous media: 3-D imaging coupled with CFD simulation, *Chem. Eng. Sci.* 63 (2008) 244–252.
- [36] M. A. Tahir, H. V. Tafreshi, S. A. Hosseini, B. Pourdeyhimi, Modeling the role of microstructural parameters in radiative heat transfer through disordered fibrous media, *Int. J. Heat Mass Transf.* 53 (2010) 4629–4637.
- [37] A. Koponen, D. Kandhai, E. Hellén, M. Alava, A. Hoekstra, M. Kataja, K. Niskanen, P. Slood, J. Timonen, Permeability of three-dimensional random fibre webs, *Phys. Rev. Lett.* 80 (4) (1998) 716–719.
- [38] A. Koponen, M. Kataja, J. Timonen, Simulations of single-fluid flow in porous media, *Int. J. Mod. Phys. C* 9 (1998) 1505–1521.
- [39] M. M. Tomadakis, T. J. Robertson, Viscous permeability of random fibre structures: Comparison of electrical and diffusional estimates with experimental and analytical results, *J. Compos. Mater.* 39 (2005) 163–188.
- [40] V. Tarnow, Calculation of the dynamic air flow resistivity of fibre materials, *J. Acoust. Soc. Am.* 102 (1997) 1680–1688.
- [41] V. Tarnow, Compressibility of air in fibrous materials, *J. Acoust. Soc. Am.* 99 (1996) 3010–3017.
- [42] V. Tarnow, Measurement of sound propagation in glass wool, *J. Acoust. Soc. Am.* 97 (1995) 2272–2281.
- [43] V. Tarnow, Fiber movements and sound attenuation in glass wool, *J. Acoust. Soc. Am.* 105 (1999) 234–240.
- [44] K. Schladitz, S. Peters, D. Reinel-Bitzer, A. Wiegmann, J. Ohser, Design of acoustic trim based on geometric modelling and flow simulation for non-woven, *Comput. Mater. Sci.* 38 (2006) 56–66.
- [45] F. P. Mechel, Ausweitung der Absorberformel von Delany and Bazley zu tiefen Frequenzen [Extending the absorption formula of Delany and Bazley to low frequencies], *Acustica* 35 (1976) 210–213.
- [46] C. Jensen, R. Raspet, Thermoacoustic properties of fibrous materials, *J. Acoust. Soc. Am.* 127 (2010) 3470–3484.
- [47] M. Küçük, Y. Korkmaz, The effect of physical parameters on sound absorption properties of natural fibre mixed nonwoven composites, *Text. Res. J.* 82 (2012) 2043–2053.
- [48] C. Peyrega, D. Jeulin, Estimation of acoustic properties and of the representative volume element of random fibrous media, *J. Appl. Phys.* 113 (2013) 104901.
- [49] C. Peyrega, D. Jeulin, Effects of the microstructure of fibrous media on their acoustic properties, in: *Proceedings of the COMSOL Conference 2010*, Paris, 2010.
- [50] D. Jeulin, Random texture models for materials structures, *Stat. Comput.* 10 (2000), 121–131.
- [51] ISO 10534-2: *Determination of sound absorption coefficient and impedance in impedance tubes*, International Organisation for Standardization, 1998.
- [52] R. J. S. Brown, Connection between formation factor for electrical resistivity and fluid-solid coupling factor in Biot’s equations for acoustic waves in fluid-filled porous media, *Geophysics* 45 (1980) 1269–1275.
- [53] T. G. Zieliński, Pore-size effects in sound absorbing foams with periodic microstructure: modelling and experimental verification using 3D printed specimens, in: P. Sas, D. Moens, A. van de Walle (Eds.), *Proceedings of ISMA2016 International Conference on Noise and Vibration Engineering and USD2016 International Conference on Uncertainty in Structural Dynamics*, 2016, pp. 95–104.
- [54] T. G. Zieliński, Normalized inverse characterization of sound absorbing rigid porous media, *J. Acoust. Soc. Am.* 137 (2015) 3232–3243.
- [55] V. Tarnow, Measured anisotropic air flow resistivity and sound attenuation of glass wool, *J. Acoust. Soc. Am.* 111 (6) (2002) 2735–2739.
- [56] A. H.-D. Cheng, Material coefficients of anisotropic poroelasticity, *Int. J. Rock Mech. Min. Sci.* 34 (1997) 199–205.
- [57] H. J. Rice, P. Göransson, A dynamical model of light fibrous materials, *Int. J. Mech. Sci.* 41 (1999) 561–579.
- [58] S. C. Cowin, Anisotropic poroelasticity: fabric tensor formulation, *Mech. Mater.* 36 (2004) 665–677.
- [59] P. J. Matuszyk, L. F. Demkowicz, Solution of coupled poroelastic/acoustic/elastic wave propagation problems using automatic hp-adaptivity, *Comput. Methods Appl. Mech. Engrg.* 281 (2014) 54–80.
- [60] J. P. Parra Martinez, O. Dazel, P. Göransson, J. Cuenca, Acoustic analysis of anisotropic poroelastic multilayered systems, *J. Appl. Phys.* 119 (2016) 084907.